Developmental Cell
Article

Coordinated Lumen Contraction and Expansion during Vulval Tube Morphogenesis in *Caenorhabditis elegans*

Sarfarazhussain Farooqui,[1,2] Mark W. Pellegrino,[1,3] Ivo Rimann,[1,4] Matthias K. Morf,[1,2] Louisa Müller,[1] Erika Fröhli,[1] and Alex Hajnal[1,*]

[1]University of Zürich, Institute of Molecular Life Sciences, Winterthurerstrasse 190, CH-8057, Switzerland
[2]Molecular Life Sciences PhD Program, Uni ETH Zürich, CH-8057, Switzerland
[3]Present address: Memorial Sloan Kettering Cancer Center, Rockefeller Research Laboratories, RRL 617B, 430 East 67th Street, New York, NY 10065, USA
[4]Present address: The Scripps Research Institute, 10550 North Torrey Pines Road, La Jolla, CA 92037, USA
*Correspondence: alex.hajnal@imls.uzh.ch
http://dx.doi.org/10.1016/j.devcel.2012.06.019

SUMMARY

Morphogenesis is a developmental phase during which cell fates are executed. Mechanical forces shaping individual cells play a key role during tissue morphogenesis. By investigating morphogenesis of the *Caenorhabditis elegans* hermaphrodite vulva, we show that the force-generating actomyosin network is differentially regulated by NOTCH and EGFR/RAS/MAPK signaling to shape the vulval tube. NOTCH signaling activates expression of the RHO kinase LET-502 in the secondary cell lineage through the ETS-family transcription factor LIN-1. LET-502 induces actomyosin-mediated contraction of the apical lumen in the secondary toroids, thereby generating a dorsal pushing force. In contrast, MAPK signaling in the primary lineage downregulates LET-502 RHO kinase expression to prevent toroid contraction and allow the gonadal anchor cell to expand the dorsal lumen of the primary toroids. The antagonistic action of the MAPK and NOTCH pathways thus controls vulval tube morphogenesis linking cell fate specification to morphogenesis.

INTRODUCTION

Organogenesis requires the differentiation of selected cells followed by tissue morphogenesis, which involves cell shape changes, cell-cell interactions, and coordinated cell movements. Tubes are the basic building blocks of most epithelial organs. Tube morphogenesis is therefore an essential process in various developmental processes such as embryonic development, tissue vascularization, and the development of most epithelial organs (Andrew and Ewald, 2010; Rodríguez-Fraticelli et al., 2011). During tissue morphogenesis, mechanical forces generated between cells are necessary to determine the proper size and shape of an organ. With a high degree of mechanical coupling between cells, tissue morphogenesis could be governed by forces from a few cells pushing or pulling all other cells (Gov, 2007). Major challenges are therefore to identify the cells that exert physical forces and the molecular pathways that control the generation of forces. In vivo models used to address these questions include vascular sprouting and branching in vertebrates, neuroblast migration during lateral line formation in the Zebrafish embryo, border cell migration in *Drosophila* ovaries, and tracheal morphogenesis in the *Drosophila* embryo (Rodríguez-Fraticelli et al., 2011; Schottenfeld et al., 2010). In most cases, "leader cells" at the front of an advancing group of cells generate forces that are transmitted rearward from cell to cell and thus act to pull along the "follower cells" (Gov, 2007; Omelchenko et al., 2003; Poujade et al., 2007; Vaughan and Trinkaus, 1966). However, forces that arise predominately within follower cells and extend over several cell rows to cells at the leading edge have been observed during the collective migration of cultured MDCK cells (Xavier Trepat et al., 2009).

Here, we are investigating morphogenesis of the *Caenorhabditis elegans* hermaphrodite vulva, a tubular organ that connects the uterus to the outside and permits egg laying. While the molecular mechanisms that regulate cell fate specification during vulval induction have been characterized in great detail, much less is known about the signaling pathways controlling vulval morphogenesis (Sternberg, 2005). During vulval induction, the interplay between the EGFR/RAS/MAPK and NOTCH pathways determines the two vulval cell fates. The gonadal anchor cell (AC) induces the primary (1°) cell fate in the adjacent vulval precursor cell (VPC) P6.p by activating the EGFR/RAS/MAPK pathway. High levels of MAPK activity in P6.p result in the phosphorylation and inactivation of the LIN-1 ETS transcription factor that represses 1° cell fate specification in the remaining VPCs (Beitel et al., 1995). P6.p then induces via a lateral DELTA/NOTCH signal the neighboring VPCs P5.p and P7.p to adopt the secondary (2°) cell fate (Greenwald, 2005). The three induced VPCs—P5.p, P6.p, and P7.p—go through three rounds of cell divisions to generate 22 vulval cells with seven distinct subfates. The seven descendants of each P5.p and P7.p adopt the VulA, VulB1, VulB2, VulC, and VulD subfates, while the eight 1° descendants of P6.p adopt the VulE and VulF subfates (Figure 1I) (Sharma-Kishore et al., 1999). During the subsequent phase of morphogenesis, the vulval cells invaginate and move dorsal (i.e., from the ventral midline toward the dorsal uterus) to form the vulval lumen. At the same time, the cells extend

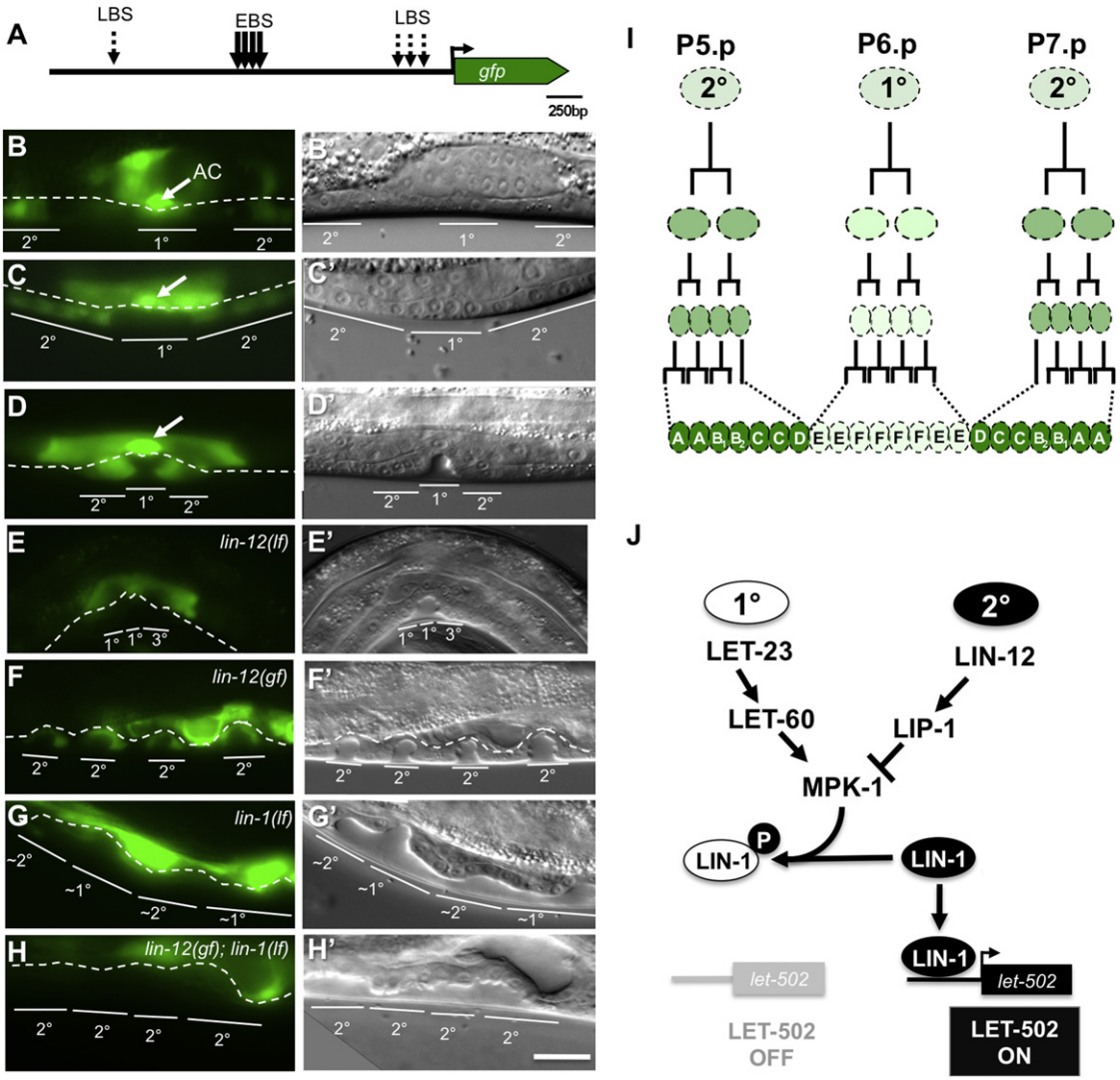

Figure 1. LIN-12 NOTCH Induces LET-502 Expression in the 2° Vulval Lineage via LIN-1 ETS

(A) Structure of the transcriptional $P_{let\text{-}502}$*::gfp* reporter. The locations of the four LBS and EBS sites are indicated.

(B–H') Time-course analysis of $P_{let\text{-}502}$*::gfp* expression from the L2 until the L4 stage with, in (B') through (D'), the corresponding Nomarski images. (E) $P_{let\text{-}502}$*::gfp* expression and (E') the corresponding Nomarski image in *lin-12(lf)*, (F and F') *lin-12(gf)*, (G and G') *lin-1(lf)*, and (H and H') *lin-12(gf); lin-1(lf)* mutants. In all panels, anterior is to the left and ventral is to the bottom, and the dotted lines represent the uterine-vulval boundary. Scale bar, 5 μm.

(I) Summary of the *let-502* expression pattern in the vulval cell lineage. The VulA through VulF subfates are indicated.

(J) Model for the transcriptional regulation of *let-502* by LIN-12, LET-23 EGFR, MPK-1 MAPK, and LIN-1. Alleles used: *lin-12(n137 gf)*, *lin-12(n137 gf n720lf)*, *lin-1(n301)*, and *sls1078*.

circumferentially toward the vulval midline, where they make homotypic contacts with their contralateral partner cells of the same subfate, thereby forming seven concentric epidermal rings called *vulval toroids* (Figure 7K). In a final step, the AC expands the dorsal lumen of VulF (Estes and Hanna-Rose, 2009) and fuses with the uterine-seam cell (utse) syncytium.

We have found that NOTCH signaling in the 2° cells positively regulates via the LIN-1 transcription factor expression of the Rho-kinase LET-502, which induces a contractile force on the apical surface of the 2° toroids and thereby generates a dorsal pushing force. EGFR/RAS/MAPK signaling, on the other hand, prevents contraction of the 1° toroids by repressing LET-502 expression, allowing the AC to expand the 1° toroid lumen and connect the toroids to the uterus. Thus, the antagonistic NOTCH and RAS/MAPK signaling pathways coordinate actomyosin-induced forces to shape the toroids.

RESULTS

LET-502 Is Differentially Expressed in the 1° and 2° Vulval Cell Lineages

We identified *let-502*, which encodes a Rho-activated kinase (Wissmann et al., 1997), as a gene specifically expressed in the 2° vulval lineage in an in silico screen for genes containing at

least three conserved LAG-1 binding sites (LBSs) (Christensen et al., 1996) in their regulatory regions (dashed arrows in Figure 1A) (S.F. and A.H., unpublished data). To analyze the expression pattern of *let-502* during vulval development, we examined the expression of a $P_{let\text{-}502}$*::gfp* transcriptional reporter containing 2.8 kilobase (kb) pairs upstream of the *let-502* translational start site fused to a *gfp* cassette (a kind gift of the *C. elegans* Gene Expression Consortium). $P_{let\text{-}502}$*::gfp* was expressed at equal levels in P3.p–P8.p before vulval induction in early to mid-L2 larvae (Figure 1B; data not shown). During vulval induction, $P_{let\text{-}502}$*::gfp* was downregulated in the 1° descendants of P6.p, while expression gradually increased in the P5.p and P7.p descendants that form the 2° lineage (Figures 1C and 1I). *let-502* expression peaked at the onset of vulval morphogenesis, when highest expression was observed in the 2° cells (Figures 1D and 1I; Figure S1A available online). Thus, *let-502* transcription is upregulated in the 2° cells and downregulated in the 1° cells after the vulval cell fates have been specified.

LET-502 Expression Is Regulated by LIN-12 NOTCH Signaling via LIN-1 ETS

Since the 2° lineage-specific expression of *let-502* is characteristic of LIN-12 target genes, we tested if LIN-12 controls *let-502* transcription. $P_{let\text{-}502}$*::gfp* was expressed in the ectopic 2° cells induced in *lin-12(gf)* mutants, while vulval *let-502* expression was absent in *lin-12(lf)* mutants, in which P5.p and P7.p adopt the 1° or 3° instead of the 2° cell fate (Figures 1E and 1F) (Greenwald, 2005). To test if LIN-12 directly regulates *let-502* transcription, we created the $P_{let\text{-}502}$ *ΔLBS::gfp* reporter, in which all four LBSs had been mutated from RTGGGAA to RAGGGAA. Surprisingly, the $P_{let\text{-}502}$ *ΔLBS::gfp* mutant reporter did not show any change in the expression pattern (Figure 2A; Figure S1B), suggesting that *let-502* is an indirect LIN-12 target. Deletion analysis of the *let-502* regulatory region identified an enhancer element required for 2°-specific expression in a 300 bp region between positions −1800 and −1400 containing a cluster of four putative ETS binding sites (EBS) defined by the motif $GGA^{A}/_{T}$ (Figure 2A) (Sementchenko and Watson, 2000; Zhang and Greenwald, 2011). The *lin-1* gene encodes an ETS family transcription factor that was originally identified as a repressor of vulval development (Beitel et al., 1995). We thus examined *let-502* expression in *lin-1(n304lf)* mutants, in which all six VPCs adopt an alternating pattern of 1° and 2° cell fates. Even though P5.p and P7.p execute a normal 2° cell lineage in *lin-1(lf)* mutants, no vulval expression of the $P_{let\text{-}502}$*::gfp* reporter was observed in *lin-1(lf)* mutants (Figure 1G). To determine the epistatic relationship between *lin-12* and *lin-1*, we analyzed $P_{let\text{-}502}$*::gfp* expression in *lin-12(gf); lin-1(lf)* double mutants, in which all VPCs adopt a 2° cell fate. Similar to *lin-1(lf)* single mutants, no vulval $P_{let\text{-}502}$*::gfp* expression was detected in *lin-12(gf); lin-1(lf)* double mutants (Figure 1H), indicating that LIN-12 regulates *let-502* expression indirectly via LIN-1. Since LIN-1 activity is negatively regulated by MAPK phosphorylation in 1° cells and LIN-12 signaling blocks MAPK activation in 2° cells by inducing inhibitors of the RAS/MAPK pathway such as the MAPK phosphatase LIP-1 (Berset et al., 2001; Greenwald, 2005), we hypothesized that the nonphosphorylated form of LIN-1 may act downstream of LIN-12 as a positive regulator of *let-502* transcription in the 2° cell lineage (Figure 1J).

The Nonphosphorylated Form of LIN-1 Activates *let-502* Transcription in the 2° Vulval Cells

To test the model shown in Figure 1J, we generated the $P_{let\text{-}502}$ *ΔEBS::gfp* reporter, in which the four putative EBS were deleted (Figure 2A). In two of three transgenic $P_{let\text{-}502}$ *ΔEBS::gfp* lines, no reporter expression was detected in the vulval cells, and a third line showed weak expression (Figures 2A and S1C). We then examined whether LIN-1 binds to the *let-502* enhancer region by performing chromatin immunoprecipitation (ChIP) experiments (Mukhopadhyay et al., 2008). Since LIN-1 activity is negatively regulated by MPK-1-mediated phosphorylation at the C terminus, we generated a nonphosphorylatable version of LIN-1 by truncating 90 amino acids from the C terminus, analogous to the mutation in the *lin-1(e1790)* gain-of-function allele (Jacobs et al., 1998). This constitutively active LIN-1 (LIN-1ΔCT) was tagged with hemagglutinin-streptavidin (HA) at the N terminus and expressed under control of the heat shock promoter (*hs::HA::lin-1ΔCT*). In *hs::HA::lin-1ΔCT* animals analyzed 4 hr after a brief heat shock by ChIP, we detected strongest binding to region B (positions −1518 to −1660 bp) that spans the four EBS and weaker binding to regions A and C (Figures 2A and 2B). In *hs::HA::lin-1ΔCT* animals that had not been heat shocked, binding to region B was still above background levels, probably because of basal activity of the heat shock promoter at the standard growth temperature (Figure 2B).

Next, we investigated whether induction of LIN-1ΔCT after cell fate specification has occurred was sufficient to induce *let-502* expression. In *hs::lin-1ΔCT;* $P_{let\text{-}502}$*::gfp* animals that had been heat shocked at the Pnp.x stage, *let-502* expression was upregulated in the 1° and 2° cells at the onset of invagination (Figures 2C and 2D). However, if LIN-1ΔCT expression was induced later during the Pn.pxx or Pn.pxxx stages, elevated *let-502* expression was only detected in the 2° toroids of L4 larvae, suggesting that, at later stages, LIN-1 is not sufficient to induce *let-502* in the 1° lineage (Figures 2E and 2F). We also examined *lin-31*, which encodes a Forkhead transcription factor that represses the 1° vulval cell fate in P6.p together with LIN-1 (Tan et al., 1998; Miller et al., 1993). *let-502* continued to be expressed in *lin-31(lf)* mutants, both in the descendants of the ectopically induced distal VPCs and in the P5.p and P7.p descendants (Figure 2G). Thus, LIN-1 does not require LIN-31 to induce *let-502* expression.

Since the MAP kinase MPK-1 inactivates LIN-1 via phosphorylation, we hyperactivated MPK-1 using a heat-shock-inducible *mpk-1* transgene (*hs::mpk-1*) to temporally control LIN-1 activity (Lackner and Kim, 1998). Consistent with the model shown in Figure 1J, an increase in MPK-1 activity at the Pn.px-to-Pnp.xx stage resulted in the loss of *let-502* expression at the late L4 (Pn.pxxx) stage (Figure 2I).

Taken together, the binding of LIN-1ΔCT to EBS sites that are required for vulval *let-502* expression and the changes in *let-502* reporter expression after activation or inactivation of LIN-1 indicate that the LIN-1 positively regulates *let-502* transcription in the 2° cell lineage.

LET-502 Is Required for Toroid Contraction during Vulval Morphogenesis

To investigate the role of LET-502 during vulval morphogenesis, we examined the apical cell junctions of the toroids using a DLG-1::RFP reporter (Diogon et al., 2007). In addition, we

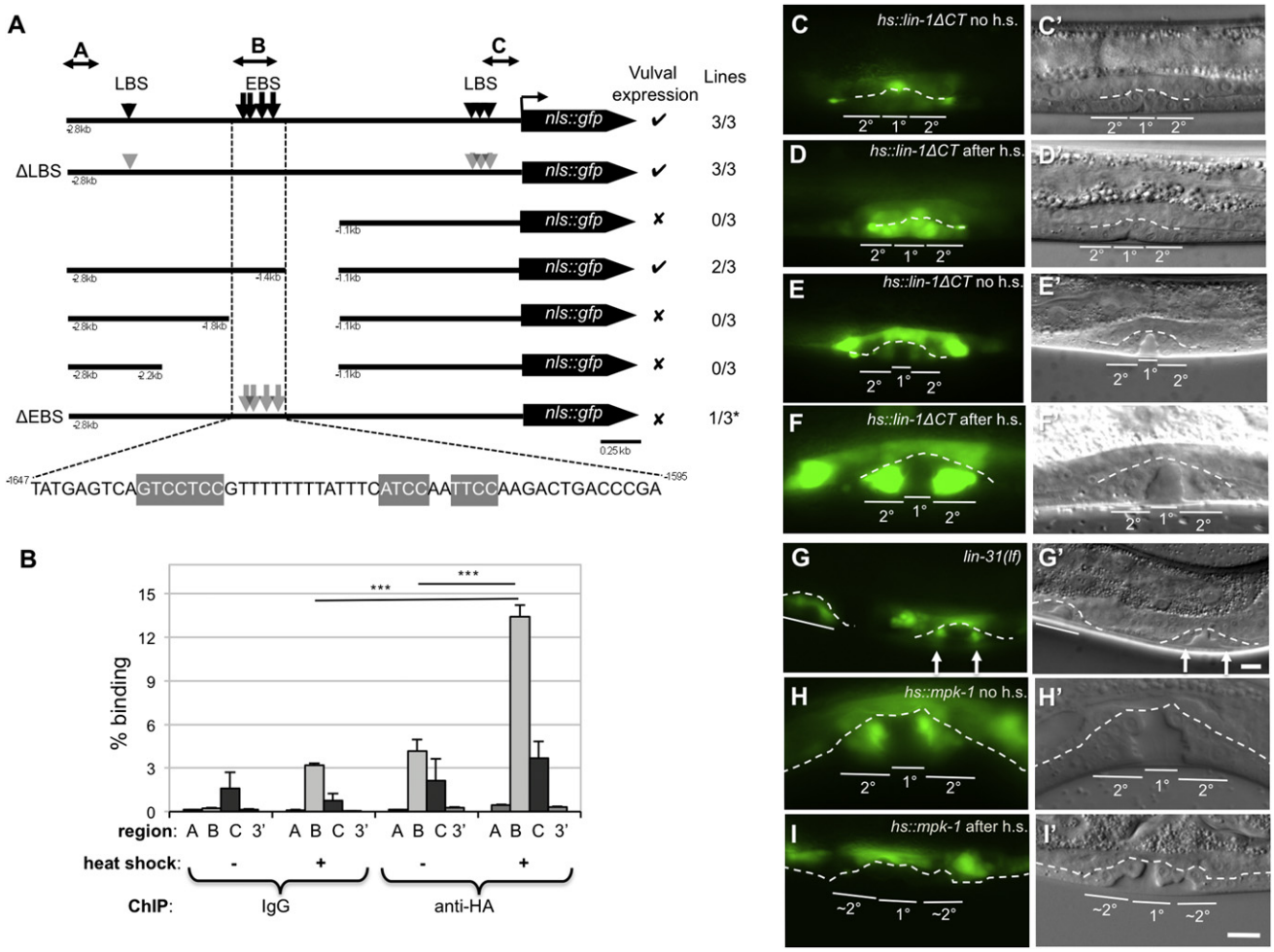

Figure 2. Nonphosphorylated LIN-1 Induces *let-502* Transcription in the 2° Vulval Cells

(A) Structure of reporter constructs used to assay *let-502* promoter activity. Three independent lines were analyzed for each construct. Arrows indicate the positions of the putative ETS binding sites (EBS) and arrowheads indicate the LAG-2 binding sites (LBS). Gray arrowheads in the ΔLBS construct indicate the point mutations changing the LBS from RTGGGAA to RAGGGAA. Grey arrows in the ΔEBS construct indicate the deletions of the EBS and the deleted nucleotides are shaded in gray. The double-headed arrows indicate regions A, B, and C used as probes for ChIP.

(B) Binding of LIN-1ΔCT to the *let-502* 5′ regulatory region detected by ChIP followed by Q-PCR. A, B, and C refer to the probe regions shown in (A) and 3′ to a probe at the 3′ end of the gene. Error bars indicate the SDs of three experiments. $^{**}p \leq 0.01$, $^{***}p \leq 0.001$, two-tailed t tests.

(C–I′) $P_{let\text{-}502}$*::gfp* expression and the (C′) corresponding Nomarski image in a *hs::lin-1ΔCT* larva at the onset of invagination (late Pn.pxx to early Pn.pxxx stage) without heat shock, and in (D) and (D′), the same stage after heat shock at the Pn.px stage. (E), (E′), (F), and (F′) show $P_{let\text{-}502}$*::gfp* expression in a *hs::lin-1ΔCT* larva at the late L4 (Pn.pxxx) stage without and after heat shock at the late Pn.pxx stage, respectively. (G) and (G′) show $P_{let\text{-}502}$*::gfp* expression in a *lin-31(lf)* L4 larva. Note that expression was detected in the P.5 and P7.p descendant (arrows) as well as in the ectopically induced P3.p and P4.p descendants (underlined). (H) and (H′) show $P_{let\text{-}502}$*::gfp* expression in a *hs::mpk-1* larva without and, in (I) and (I′) after heat shock at the Pn.pxx stage. In all panels, anterior is to the left and ventral is to the bottom, and the dotted lines represent the uterine-vulval boundary. Scale bars, 5 μm. Alleles used in (A): *zhEx393, 398, 399, 401-405*, (B): *zhEx394*, (C through I): *lin-31(n301), gaIs36, zhEx395, sIs10781*.

See also Figure S1.

visualized filamentous actin (F-actin) microfilaments (MFs) using a reporter, in which the actin-binding domain of Abp140 (first 17 amino acids) had been fused to GFP and expressed under control of the pan-epithelial *dlg-1* promoter ($P_{dlg\text{-}1}$*::LifeAct::gfp*) (Pohl and Bao, 2010).

In the 2° VulA, VulB1, and VulB2 toroids of wild-type L4 larvae, actin MFs were arranged in circumferential rings, which localized in proximity to DLG-1::RFP outlining the apical junctions on the luminal side of the toroids (Figures 3A and 3C). In contrast, the MFs in the 1° VulE and VulF toroids formed a pyramid-shaped meshwork oriented along the dorsoventral (D/V) axis, thereby connecting VulE and VulF on the dorsal side to the ventral uterus and on the ventral side to the 2° toroids. Weak LifeAct::GFP staining was also visible in the cell bodies of VulB1 and VulB2 (asterisks in Figure 3A).

We next examined the toroids in *let-502(ok1283)* null mutants, which carry a 1,435 bp deletion removing the Rho binding and pleckstrin-homology (PH) domains and causing a frameshift in the remaining exons, which results in a zygotic adult sterile phenotype as reported for other *let-502(lf)* alleles (Figure S3A)

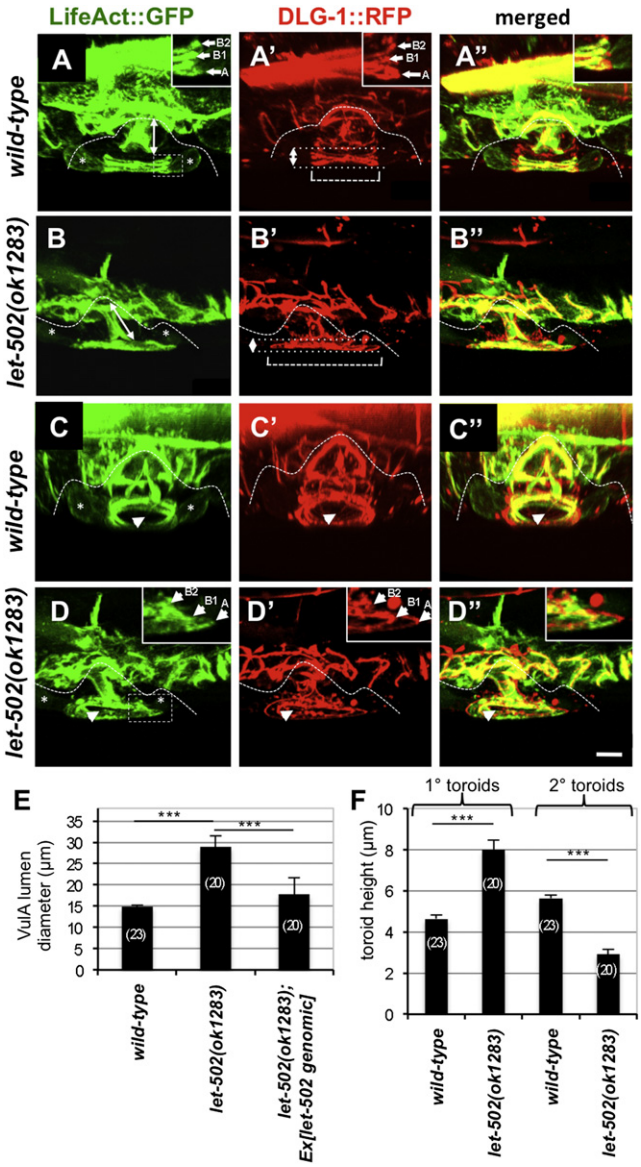

Figure 3. LET-502 Is Required for Toroid Contraction during Vulval Morphogenesis

(A–D'') 3D reconstructions of LifeAct::GFP expression to visualize polymerized actin, (A') DLG-1::RFP to visualize the apical junctions and (A'') the merged images in the toroids of a wild-type L4 and (B through B'') a *let-502(lf)* L4 larva. (C) through (D'') show ventrolateral projections of the same animals. The dashed lines in all panels indicate the uterine-vulval boundary. The double arrows in (A) and (B) indicate the height of 1° toroids, and in (A') and (B') the 2° toroid height between the dotted lines. The dashed bracket indicates the VulA lumen diameter. The dashed boxes in (A) and (D) indicate the regions magnified in the insets showing midsagittal sections. The asterisks in (A), (B), (C), and (D) indicate LifeAct staining in the cell bodies. The arrowheads in (C) through (D'') indicate the vulval lumen.

(E) Average VulA lumen diameter in wild-type, *let-502(lf)*, and *let-502(lf)* mutants rescued with a 12.8-kb *let-502* genomic fragment. For details on the measurement points used to quantify each parameter, see Figure S5.

(G) Average 1° and 2° toroid heights in wild-type and *let-502(lf)* mutants. The numbers in brackets indicate the number of animals analyzed, and the error bars indicate SDs. $^{**}p \leq 0.01$, $^{***}p \leq 0.001$, two-tailed t tests. Scale bar, 5 μm. Alleles used: *let-502(ok1283), mcIs46,* and *zhIs396*.

See also Figure S2.

(Wissmann et al., 1999). In *let-502(ok1283)* larvae, we did not observe an obvious change in cell fate marker expression (Figure S2) or the number of vulval toroids, although the overall shape of the toroids appeared to be distorted (Figures 3B and 3D). The average diameter of the 2° VulA toroid lumen diameter was increased about 2-fold, while the combined height of the 2° toroids was decreased (Figures 3E and S3A). The 1° VulE and VulF toroids, on the other hand, were stretched along the D/V axis, and their combined height was increased (Figures 3B and 3G). Moreover, actin MFs in the 2° VulA, VulB1, and VulB2 toroids of *let-502(ok1283)* mutants appeared to be slightly disorganized, even though they still formed circumferential rings (Figure 3D). A 12.8 kb genomic fragment spanning the entire *let-502* locus and including the downstream gene C10H11.8, which may be in an operon together with *let-502*, rescued the toroid morphogenesis defects of *let-502(ok1283)* mutants (Figure 3F; Figure S3A). Finally, a translational LET-502::GFP reporter showed expression near the apical lumen of the 2° toroids and weak or undetectable expression in 1° toroids (Figure S3B).

Taken together, the increased diameter and decreased height of the 2° toroids in *let-502* mutants together with the circumferential localization of actin MFs near the apical junctions of the 2° toroids suggested that actomyosin-mediated contraction on the luminal side of the 2° toroids is essential to shape the vulval toroids.

LET-502 Regulates 1° and 2° Toroid Diameters by Inducing Actomyosin Contraction

We visualized myosin MFs either by staining L4 larvae with antibodies against non-muscle myosins NMY-1 and NMY-2 (Piekny et al., 2003) or by observing expression of a myosin light chain MLC-4 reporter containing 2.83 kbp of 5′ regulatory sequences (Figure 4A; Figures S3D and S3E). Here, we observed localization of an MLC-4$R_{17}A_{18}$::GFP nonphosphorylatable mutant, although the same localization was observed with the constitutively active MLC-4$D_{17}D_{18}$ mutant (Gally et al., 2009; data not shown). MLC-4 and the nonmuscle myosins were localized similar to actin MFs near the apical junctions. However, while NMY-1 and NMY-2 were equally expressed in all toroids, MLC-4(RA)::GFP was only detected in the VulA, VulB1, and VulB2 toroids (Figure 4A). During eversion in the final phase of vulval morphogenesis, MLC-4::GFP was detected in all toroids (data not shown). Thus, the VulA, VulB1, and VulB2 toroids contain actin-myosin bundles organized in circumferential rings, while the VulC, VulD, VulE, and VulF toroids contain lower amounts of MLC-4 and no circumferential actin MFs.

Since LET-502 Rho Kinase phosphorylates MLC-4 to induce actomyosin contraction (Diogon et al., 2007), we examined whether expression of the constitutively active MLC-4DD mutant rescued the enlarged diameter of the 2° toroids in *let-502(ok1283)* mutants. Since *let-502(ok1283); mcEx402[P_{mlc-4}::mlc-4DD::gfp]* animals were inviable for unknown reasons, we used RNAi to knock down *let-502* function. While *let-502* RNAi caused approximately a 40% increase in 2° toroid diameter in nontransgenic controls, no significant increase in lumen diameter was observed in the transgenic *[P_{mlc-4}::mlc-4DD::gfp]* siblings treated with *let-502* RNAi on the same plates (Figure 4D). Thus, LET-502 induces actomyosin-mediated contraction of the 2° toroids via MLC-4.

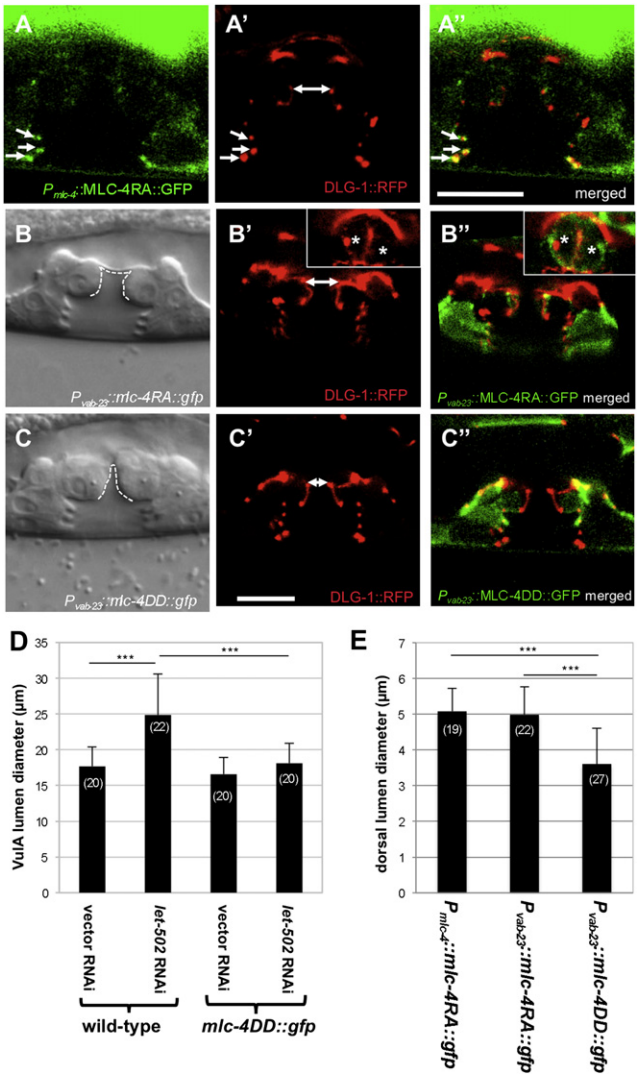

Figure 4. Localization of MLC-4 and Ectopic Expression in 1° Toroids

(A) Confocal midsagittal section of MLC-4RA::GFP (A') DLG-1::RFP and (A") the merged images in the toroids of an L4 larva. The arrows point at MLC-4RA::GFP localized near the apical junctions of the VulA, VulB1, and VulB2 toroids.

(B–B") Nomarski image of a P_{vab-23}::*mlc-4RA::gfp* L4 larva showing normal expansion of the dorsal lumen outlined with a dashed line. (B') DLG-1::RFP and (B") the merged MLC-4::GFP and DLG-1::RFP images of the same animal. The insets show an upper plane with 1° VulE and VulF toroids expressing MLC-4RA::GFP labeled with asterisks.

(C–C") Nomarski image of a P_{vab-23}::*mlc-4DD::gfp* L4 larva showing incomplete expansion of the dorsal lumen. (C') DLG-1::RFP and (C") the merged images of the same animal are shown. Scale bars, 10 µm.

(D) Average VulA lumen diameter in wild-type and *mlc-4::DD::gfp* L4 larvae treated with *let-502* RNAi or empty vector control. *mlc-4::DD::gfp* transgenic animals were compared to nontransgenic siblings on the same RNAi plates.

(E) Average dorsal lumen diameter in P_{mlc-4}::*mlc-4RA::gfp*, P_{vab-23}::*mlc-4RA::gfp*, and P_{vab-23}::*mlc-4DD::gfp* L4 larvae measured at the VulE/VulF junctions as described in Figure S5. The numbers in brackets indicate the number of animals analyzed, and the error bars indicate the SDs. p-values obtained in two-tailed t tests are indicated as $^{**}p \leq 0.01$, $^{***}p \leq 0.001$. Alleles used: *mcIs46, zhEx437, zhEx438, zhEx439*, and *mcEx402*.

See also Figures S3 and S4.

During the mid-L4 stage, the AC invades and expands the dorsal lumen formed by the 1° toroids (Estes and Hanna-Rose, 2009). We therefore examined the role of actomyosin MFs in dorsal toroid lumen expansion by expressing constitutively active MLC-4DD in the 1° VulF and VulE toroids under control the *vab-23* promoter (P_{vab-23}::*mlc-4DD::gfp*), and as negative control the nonphosphorylatable MLC-4RA mutant (P_{vab-23}::*mlc-4RA::gfp*; Figures 4B and 4C) (Pellegrino et al., 2011). The diameter of the dorsal toroid lumen in P_{vab-23}::*mlc-4DD::gfp* animals was significantly reduced compared to P_{vab-23}::*mlc-4RA::gfp* or P_{mlc-4}::*mlc-4RA::gfp* controls (Figure 4E). A similar phenotype was observed after RNAi knockdown of the *mel-11* phosphatase, which inhibits actomyosin contraction by dephosphorylating MLC-4 (Figures S3F and S4) (Wissmann et al., 1999).

We conclude that ectopic actomyosin contraction in the 1° toroids prevents proper expansion of the dorsal toroid lumen. Hence, RAS/MAPK signaling represses *let-502* expression in the 1° toroids to permit dorsal lumen expansion by the AC.

LIN-1 Regulates Multiple Aspects of Vulval Morphogenesis

Since LIN-1 directly activates *let-502* transcription in the 2° vulval cells, we examined if loss of *lin-1* function may cause similar vulval morphogenesis defects as *let-502(lf)*, in addition to the ectopic vulval induction caused by loss of the inhibitory LIN-1 function during fate specification. We first examined vulval toroid formation in *lin-1(n304lf)* mutants at the L4 stage by staining the apical junction marker AJM-1. Although P5.p, P6.p, and P7.p adopt a normal 2°-1°-2° pattern of cell fates based on cell lineage analysis (Beitel et al., 1995), their descendants failed to form ring-like structures characteristic of vulval toroids (Figure 5B). Instead, the vulval cells retained a square shape and failed to extend the circumferential processes containing actin bundles that were observed in the wild-type (Figure 5F). In contrast, in animals carrying a gain-of-function mutation in *let-60 ras*, P5.p, P6.p, and P7.p formed toroids with a similar morphology as in the wild-type (Figure 5C) (Sharma-Kishore et al., 1999), indicating that hyperactivation of the RAS pathway per se does not disrupt vulval morphogenesis.

To further investigate the role of LIN-1 during vulval morphogenesis, we inactivated LIN-1 after vulval fate specification by providing a pulse of MPK-1 activity in all vulval cells. When *hs::mpk-1* animals were heat shocked at the Pnp.xx-Pnp.xxx stage (Figure 5A), we observed not only a loss of *let-502* expression as shown in Figure 2I but also an abnormal toroid formation (Figure 5E). Except for the VulF cells, no toroid-like structures were formed by the P5.p, P6.p, and P7.p descendants at the L4 stage, similar to *lin-1(n304)* mutants. Moreover, the diameter of the vulval lumen was increased to a similar extent as in *let-502(ok1283)* mutants (Figure 5G).

Thus, inactivation of LIN-1 after vulval induction almost completely disrupts vulval toroid formation, suggesting that LIN-1 regulates vulval morphogenesis by controlling additional target genes besides *let-502*.

Contraction of the 2° Toroids and Expansion of the 1° Toroids by the AC Shape the Vulval Tube

The increased lumen diameter and reduced height of the 2° toroids in *let-502* mutants suggested that the contraction of

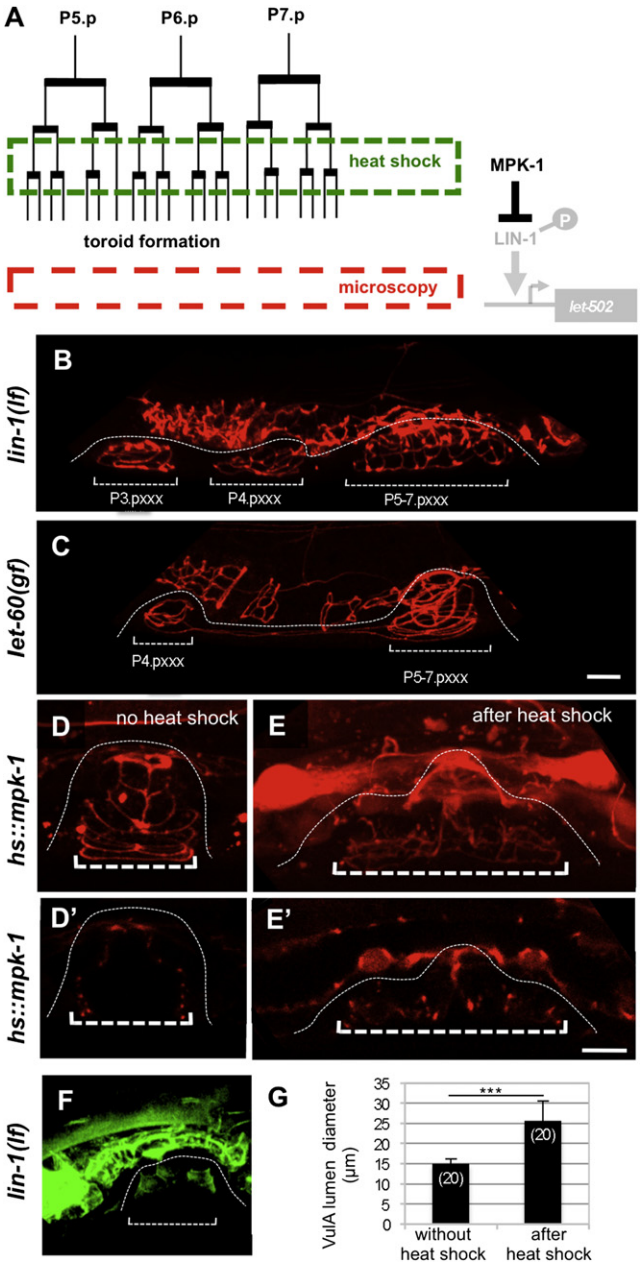

Figure 5. LIN-1 Regulates Multiple Aspects of Vulval Morphogenesis

(A) Lineage diagram showing the timing of *mpk-1* induction by heat shock and observation by 3D microscopy.

(B and C) Vulval toroid junctions visualized by MH27 antibody staining in (B) a *lin-1(lf)* and (C) a *let-60(gf)* mutant L4 larva.

(D–E') Vulval toroid junctions at the L4 stage visualized by DLG-1::RFP expression (D) without and (E) after heat shock induction of MPK-1 at the Pn.pxx stage. (D') and (E') show midsagittal sections of the animals shown in (D) and (E), respectively.

(F) Polymerized actin visualized with LifeAct::GFP expression in a *lin-1(lf)* L4 larva. Note the absence of circumferential actin rings formed in 2° cells as shown for the wild-type in Figure 3A. The dashed lines indicate the vulval-uterine boundary and the dashed brackets the diameters of the multiple invaginations. Scale bars, 5 µm.

(G) Average VulA diameter without and after heat-shock induction of MPK-1 measured as described in Figure S5. The numbers in brackets indicate the number of animals analyzed, and the error bars indicate the SDs.

the 2° toroids might generate a dorsal (i.e., from ventral toward dorsal) pushing force during vulval invagination. To test this hypothesis, we performed cell ablation experiments removing the 2° descendants of P5.p and P7.p at the Pn.pxx stage before the onset of vulval invagination. Ablation of the 2° vulval cells alone did not block invagination of the remaining 1° cells but rather caused an increase in the height of the 1° toroids (Figures 6B and 6E; n = 11). The residual invagination and increased height of the 1° toroids in the absence of 2° cells suggested the existence of tension created by the attachment of the dorsal toroids to the uterus. We therefore ablated the AC before the onset of invagination at the Pn.pxx stage. AC ablation prevented dorsal lumen expansion and caused an increase of the 1° and a simultaneous decrease of the 2° toroid height despite the normal contraction of the 2° toroids (Figures 6C and 6E; n = 10). Interestingly, AC ablation increased the height of the 1° VulF but not the VulE toroid, while ablation of the 2° cells increased the height of both the VulF and VulE toroids (Figure 6F). Finally, simultaneous ablation of the AC and the 2° cells resulted in the formation of a very small vulval lumen without a connection between the uterus and the cuticle (Figure 6D; n = 10). The height of the remaining 1° toroids could not be reliably quantified due to their small size and severely distorted morphology. Taken together, the ventral contraction of the 2° toroids by the actomyosin MFs and the lateral expansion of the 1° toroids by the AC are both required to shape the vulval tube and form a normal invagination.

Quantitative Analysis of Shape Changes during Toroid Morphogenesis

To quantify the dynamic shape changes of the toroids, we followed vulval morphogenesis in wild-type L4 larvae expressing the apical junction marker AJM-1::GFP (Köppen et al., 2001) by time-lapse (four-dimensional; 4D) microscopy and measured the changes in toroid diameter and height over time. As the diameter of the ventral-most VulA toroid lumen decreased to its final size of less than 15 µm, the height of the 2° toroids increased, while 1° toroid height remained more or less constant (Figures 7A, 7F, and 7G; Movie S1). After the 2° toroids had fully contracted in mid-L4 larvae, we observed how the invading AC expanded the diameter of the dorsal toroid lumen (Figures 7B and 7H; Movie S1). The height of the 2° toroids further increased during this final phase of dorsal toroid lumen expansion (Figure 7I). In AC-ablated animals, on the other hand, the dorsal toroid lumen did not expand and the 1° toroid lumen remained small (Figure 6C). We also observed the vulval cell bodies during ventral lumen contraction and dorsal lumen expansion using a CED-10::GFP reporter, which labels the plasma membranes (Lundquist et al., 2001). Despite the changes in lumen size, the positions of the vulval cell bodies during ventral toroid contraction and dorsal expansion remained constant relative to the uterine cells (Movie S2; data not shown), indicating that vulval invagination is driven predominantly by changes in toroid shape rather than by active cell migration.

**$p \leq 0.01$, ***$p \leq 0.001$, two-tailed t tests. Alleles used: *lin-1(n301), mcIs46, gaIs36*, and *zhIs96*.

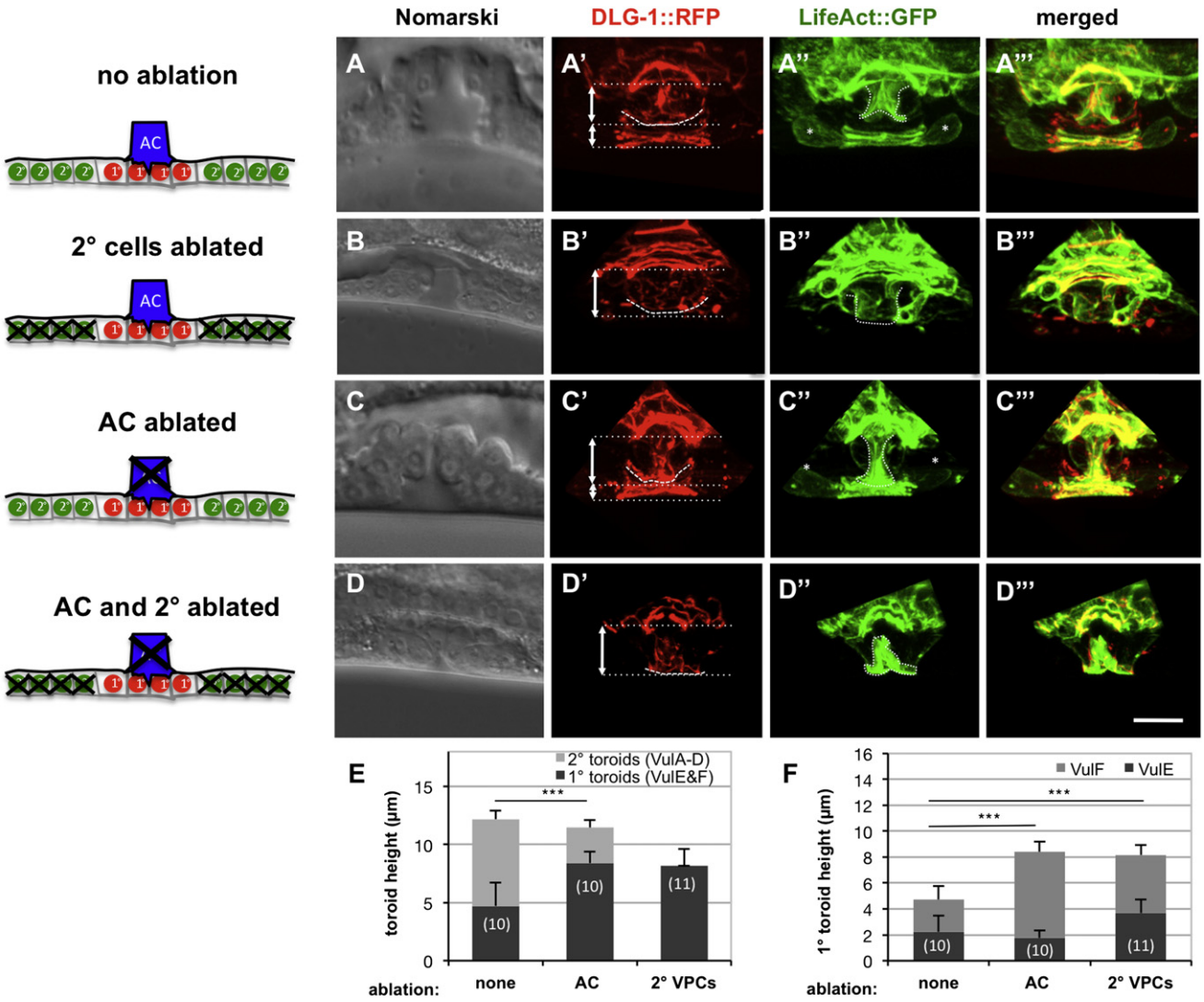

Figure 6. 2° Toroid Contraction and 1° Toroid Expansion Shape the Vulval Tube

(A–D"') (A–A"') Nomarski image, DLG-1::RFP-labeled junctions, polymerized actin visualized with LifeAct::GFP, and merged images in a wild-type L4 larva at the Pn.pxxx stage without ablation, (B–B"') after ablation of the 2° P5.p and P7.p descendants at the Pn.pxx stage, (C–C"') after ablation of the AC at the Pn.pxx stage, and (D–D"') after simultaneous ablation of the AC and the 2° P5.p and P7.p descendants. Double-headed arrows and the dotted lines indicate the height of the 1° and 2° toroids. Dashed curved lines indicate the junction between VulD and VulE or, in (B) and (D), the ventral epidermis and VulE. Scale bar, 5 µm.

(E and F) (E) Average height of the 1° and 2° toroids and (F) VulF and VulE after the different ablations measured as described in Figure S5. The numbers in brackets indicate the number of animals analyzed, and the error bars indicate the SDs. The p values obtained in two-tailed t tests comparing 2° toroid heights in (E) and 1° toroid heights in (F) are indicated as **p ≤ 0.01 and ***p ≤ 0.001. Alleles used: *mcIs46* and *zhIs396*.

Based on the dynamic changes in toroid height and diameter, we conclude that ventral 2° toroid contraction followed by lateral expansion of the 1° toroids are both required to achieve the proper height of the vulval toroids (Figure 7K).

The Ventral Toroids and the AC/Utse Syncytium Create Tension in the Toroids

Finally, we investigated the tensions as an estimate for the forces generated during toroid morphogenesis by measuring toroid recoil velocities in laser-cutting experiments. First, we tested whether the vulval lumen in L4 larvae represents a closed compartment, to which pressure is being applied during morphogenesis. For this purpose, we punctured the ventral epidermis separating the vulval lumen from the outside. This intervention caused a rapid efflux of fluids and a ventral recoil of the toroids (Figure 7C; Movie S3). The morphology of the vulva after this induced collapse of the lumen was remarkably similar to the vulva in young adult animals after vulval eversion had occurred. As an estimate for the forces involved, we measured the peak recoil velocity of the VulD toroids (Figures 7C and 7J). Next, we cut the ventral VulA, VulB1, and VulB2 toroids, which caused an instant ventral recoil of the remaining toroids, indicating that ventral toroid contraction provides support for the remaining dorsal toroids (Figure 7D; Movie S4). In the presence

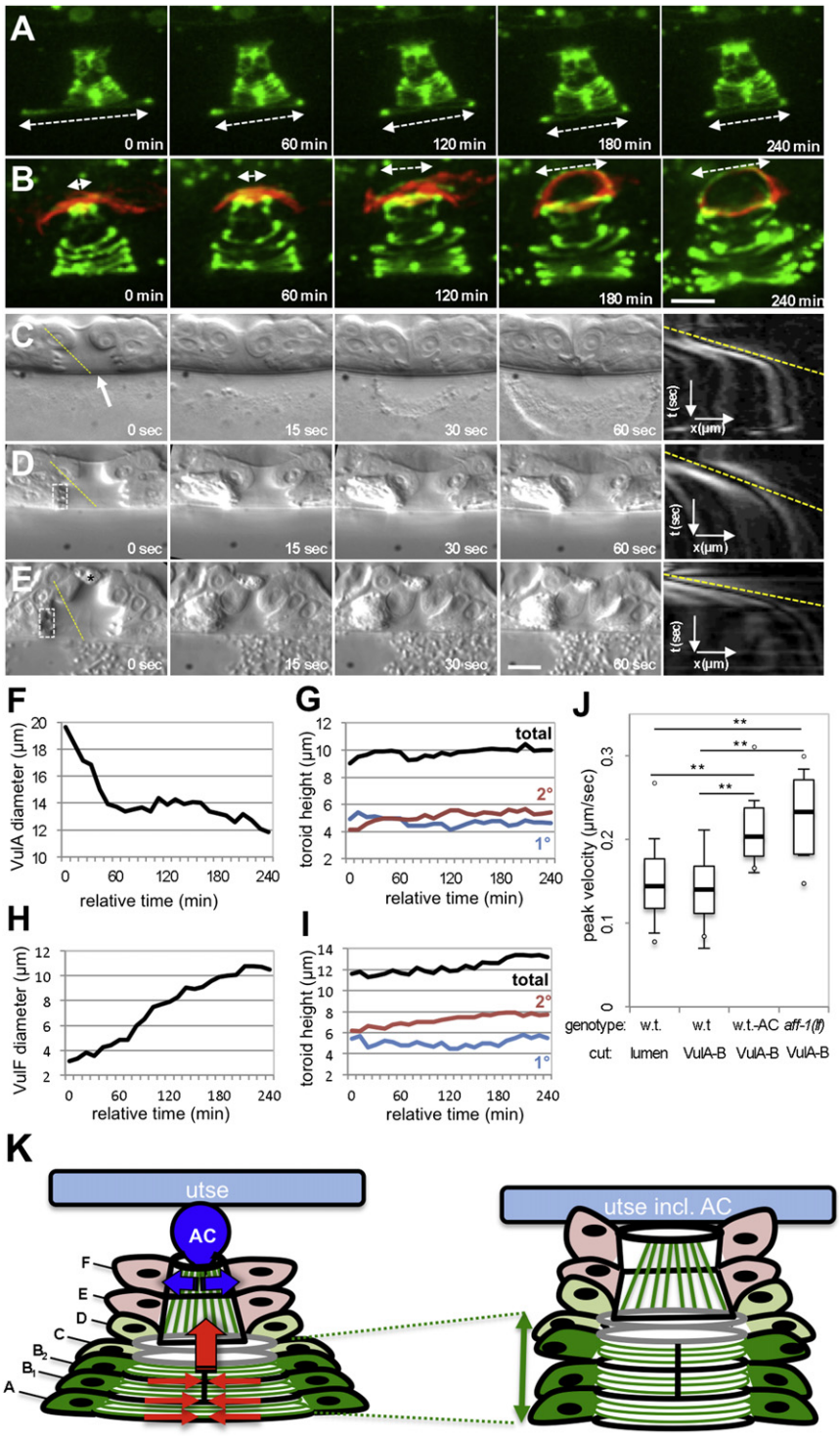

Figure 7. Quantitative Analysis of Vulval Toroid Morphogenesis

(A) Time-lapse recording of 2° toroid contraction in an early L4 larva using the AJM-1::GFP marker in green (Movie S1).

(B) Time-lapse recording of 1° toroid expansion in an L4 larva after the 2° toroids had contracted (Movie S1). The ventral plasma membrane of the AC is labeled in red using a PLC∂PH::mCherry marker (Ziel et al., 2009).

(C) Puncturing of the vulval lumen in L4 larvae results in a rapid lumen collapse and vulval eversion (Movie S3). The arrow in the first frame indicates the site in the ventral epidermis where the lumen was laser punctured. The animals were mounted in a suspension of 100 nm latex beads to visualize the efflux of fluids.

(D and E) Cutting of the VulA, VulB1, and VulB2 toroids in the (D) presence and (E) absence of the AC (Movie S4). The dashed box in the first frames outline the regions where the toroids were cut and the asterisk in (E) labels the AC corpse. The yellow dashed lines indicate the axes of VulD movement used to generate the kymograph shown in the rightmost panels and measure the peak recoil velocities. Scale bars, 5 µm.

(F and G) Quantification of the reduction in VulA (F) lumen diameter and (G) toroid height during 2° toroid contraction in the animal shown in (A).

(H and I) Quantification of the increase in VulF lumen diameter (H) and toroid height (I) during dorsal toroid lumen expansion in the animal shown in (B). Measurements on the recordings shown in (A) and (B) were performed on one out of three to five movies obtained for each stage as described in Figure S5.

(J) Box plot of the peak velocities measured in the lumen puncturing and toroid cutting experiments. The numbers in brackets indicates the number of animals analyzed, and the error bars indicate the SDs. **p ≤ 0.01, ***p ≤ 0.001, two-tailed t tests.

(K) Toroid contraction and expansion during vulval morphogenesis. Cell bodies of 1° VulF and VulE toroids are shown in light red, cell bodies of 2° VulD and VulC toroids in light green, and of VulB2, VulB1, and VulA in dark green. Green lines indicate actomyosin MFs and black and gray lines the apical cell junctions. LET-502-mediated apical contraction of VulA, VulB, and VulB2 toroids result in a dorsal pushing force (red arrows), while invasion of the AC (dark blue) into the 1° toroids laterally expands the dorsal toroid lumen (blue arrows). Finally, the AC fuses with the utse (light blue) allowing the attachment of the toroids to the utse. Alleles used: *aff-1(ty4), swIs79*, and *qyIs23*.

of the AC, we measured a similar recoil velocity as in the lumen-puncturing experiments (Figures 7D and 7J). However, if the AC was ablated at the early Pn.pxxx stage at the onset of dorsal toroid expansion, after the π cells had been specified, the recoil velocity after toroid cutting was increased by around 50% (Figures 7E and 7J; Movie S4). To further dissect the role of the AC in toroid morphogenesis, we measured recoil velocities in *aff-1(ty4)* mutants, in which the AC normally expands the dorsal lumen but does not fuse with the overlying utse syncytium formed by eight π cells (Sapir et al., 2007). Dorsal lumen diameter in *aff-1(ty4)* was 5.1 ± 1.0 µm and 5.0 ± 0.69 µm in the wild-type; n = 20 each. We observed a similar increase in recoil velocity in *aff-1(ty4)* mutants as in AC-ablated wild-type animals (Figure 7J; Movie S4).

We conclude that actomyosin-driven contraction of the 2° toroids first generates a dorsal pushing force. Then, dorsal toroid expansion followed by fusion of the AC to the utse allows the formation of a continuous connection between the dorsal toroids, the uterine uv1 cells, and the utse/AC syncytium, which anchors the toroids to the lateral seam cells and thereby generates a tension in the dorsal toroids (Figure 7K) (Lints and Hall, 2009).

DISCUSSION

LIN-1 Links Cell Fate Specification with Morphogenesis

Our data point at a direct link between the cell fate specification pathways determining the 1° and 2° vulval fates and the force-generating actomyosin network during vulval morphogenesis. Rho kinase *let-502* transcription is directly induced by the ETS-family transcription factor LIN-1 (Figure 1J). High levels of NOTCH signaling in the 2° vulval cells prevent activation of the MAPK and thus keep LIN-1 in its active, unphosphorylated state, while high levels of MAPK signaling in the 1° cells result in the phosphorylation and inactivation of LIN-1. In this manner, a differential expression of RHO kinase LET-502 is established during the subsequent phase of vulval morphogenesis, such that high levels of LET-502 are maintained in the 2° cells, whereas LET-502 expression gradually fades in the 1° cells. In contrast to LET-502, the RHO-1 GTPase and the RHO guanine exchange factor ECT-2 (S. Canevascini and A.H., unpublished data), as well as the MEL-11 phosphatase, are uniformly expressed in 1° and 2° vulval toroids, suggesting that LET-502 is a limiting factor necessary to overcome the inhibitory activity of MEL-11 and induce actomyosin contraction. Our results also indicate that continuous RAS/MAPK and NOTCH signaling are required to maintain the differential LET-502 expression, as activation or inactivation of LIN-1 after vulval fate specification altered LET-502 expression levels and perturbed vulval morphogenesis. Hence, expression of both the EGFR ligand by the AC and the NOTCH ligands by the 1° vulval cells are maintained until the final stage of vulval development.

It has recently been reported that RAS and NOTCH signaling regulate different steps in the development of the *C. elegans* excretory system (Abdus-Saboor et al., 2011). Also in this organ, RAS and NOTCH signaling control not only the specification of the different cell fates but also the morphogenesis of the excretory tube. However, the target genes regulated by LIN-1 during excretory tube morphogenesis are not known.

Interestingly, LIN-1 appears to control multiple aspects of vulval morphogenesis besides regulating LET-502 expression and independent of its earlier inhibitory role during VPC fate specification. Even though the VPCs in *lin-1(lf)* mutants adopt an alternating pattern of 1° and 2° cell fates (Beitel et al., 1995), vulval toroids are largely absent and actin MFs do not organize in circumferential bundles in the 2° toroids. Therefore, LIN-1 appears to be necessary for the formation of circumferential cell extensions and homotypic cell contacts during vulval toroid formation. The opposing effects of the NOTCH and RAS/MAPK signaling pathways on LIN-1 activity thus orchestrate the cell shape changes during vulval tube formation.

Contraction of the 2° Toroids Generates a Dorsal Pushing Force

The 2° vulval toroids differ from the 1° toroids not only by higher LET-502 expression levels but also by a different orientation of the actomyosin network (Figure 7K). While actin MFs are organized in circumferential bundles near the apical surface of the 2° VulA, VulB1, and VulB2 toroids, actin MFs in the 1° VulE and VulF toroids are aligned along the dorsoventral axis. Moreover, the regulatory myosin light chain MLC-4 was detected exclusively near the apical junctions of the 2° VulA, VulB1, and VulB2 toroids. Thus, only the three ventral-most toroids are capable of contracting in response to LET-502 activation, while the MLC phosphatase MEL-11 prevents contraction of the remaining toroids. It is not known how the different orientation of the actin fibers in 1° and 2° toroids is established. However, loss of *let-502* function did not change the overall orientation or organization of actin MFs.

The generation of a dorsal pushing force by 2° toroid contraction requires that the vulval lumen represents a closed compartment to which pressure can be applied. Indeed, when the vulval lumen was punctured in L4 larvae, this resulted in an almost instantaneous collapse of the vulval lumen and vulval eversion, indicating that the luminal space does represent a closed compartment that is under pressure. Mutations in the *sqv* genes, which encode proteins required for the biosynthesis or secretion of glycoproteins, cause a drastic reduction in the size of the vulval lumen (Herman et al., 1999; Herman and Horvitz, 1999; Hwang et al., 2003). It was proposed that hygroscopic proteoglycans secreted into the vulval lumen cause fluids to gradually increase the volume of the lumen and build up osmotic pressure. Therefore, a reduction in the radius of the lumen on the ventral side will cause an elongation of the lumen dorsally and thereby generate a dorsal pushing force (Figure 7K).

Lateral Expansion of the 1° Toroids by the AC and Attachment to the Seam

Estes and Hanna-Rose (2009) have reported that invasion of the AC into the vulval tissue is necessary for dorsal lumen morphogenesis. We found that after the contraction of the ventral 2° toroids has been completed, the lateral expansion of the dorsal 1° toroid lumen by the invading AC is accompanied by a further increase in 2° toroid height. Accordingly, early ablation of the AC before vulval invagination (at the Pn.pxx stage) resulted not only in a reduced diameter and increased length of the 1° toroids but also a decrease in 2° toroid height. On the other hand, the diameter of the 2° toroids did not increase after AC ablation as long as the LET-502 induced actomyosin contraction was normal. Thus, AC ablation probably increases the pressure on the ventral toroids, which is counteracted by the actomyosin force. This results in the flattening of the 2° toroid and the stretching of the 1° toroid, as in the absence of the AC the 1° toroids remain attached to the basement membranes between uterus and vulva. The AC may increase the diameter of the 1° lumen by inducing lateral sliding of the basement membranes between the uterine and vulval cells (Ihara et al., 2011); it may mechanically stretch the VulF toroid or induce remodeling of the cytoskeleton in VulF through direct cell-cell interaction. In either case, continuous RAS/MAPK signaling must repress *let-502* transcription in the 1° VulE and VulF toroids to inhibit

actomyosin contraction and permit the AC to expand the dorsal lumen.

The increased toroid recoil velocity in the absence of the AC or, more specifically, in the absence of fusion between the AC and utse, points at a second function of the AC that is independent of its first role during dorsal lumen expansion, as the dorsal lumen was expanded in *aff-1(lf)* mutants. The removal of the AC through fusion may make room necessary for the attachment of the overlying utse to the dorsal toroids and the uv1 cells (Sapir et al., 2007; Lints and Hall, 2009). In this manner, AC fusion allows the establishment of a continuous connection between the vulva and the uterus to anchor the vulval toroids via the utse syncytium to the lateral epidermis, which creates a lateral tension in the dorsal toroids (Figure 7K).

Regulation of Cell Shape Changes by NOTCH and RAS Signaling

Tissue morphogenesis depends on collective cell movements and the transmission of mechanical forces between different cell types. In many examples of collective cell migration, specific leader cells have been identified that generate in response to extracellular signals a mechanical force, which is transmitted to follower cells through cell-cell interactions (Caussinus et al., 2008). For example, RAS and NOTCH signaling are interlinked in a similar fashion during *Drosophila* tracheal tube morphogenesis to regulate the ETS transcription factors Pnt and Yan and differentiate between leader and follower cells (Schottenfeld et al., 2010). However, in contrast to the *Drosophila* trachea, there exists no clear distinction between leaders and followers during *C. elegans* vulval morphogenesis since not only the AC/utse/seam cell connection but also the 2° cells contribute forces to shape the vulval tube. Finally, we show that the RAS and NOTCH signaling pathways first used to specify the vulval cell fates are again used during vulval morphogenesis to differentially regulate actomyosin activity. Vulval fate specification and morphogenesis are therefore tightly coupled processes.

EXPERIMENTAL PROCEDURES

General Methods and Strains

C. elegans strains were maintained at 20°C on standard nematode growth media as described previously (Brenner, 1974). The wild-type strain of *C. elegans* used was Bristol N2. Strains used were as follows: LGI: *dpy-5(e907), let-502(ok1283)/hT2[bli-4(e937) let(q782) qIs48] (I;III)*, LGII: *aff-1(ty4), unc-4(e120), LGIII: dpy-19(e1259), lin-12(n137)/unc-32(e189) lin-12(n137n720), lin-1(n304), lin-31(n301)*, LGIV: *let-60(n1046)*. Extrachromosomal and integrated arrays: *gaIs36[hs::mpk-1(+), Dmek-2(wt)]* (Lackner and Kim, 1998), *swIs79[ajm-1::gfp,P_{scm-1}::gfp, unc-119(+)], mcIs46[dlg-1::rfp, unc-119(+)]* (Diogon et al., 2007), *sIs10781[rcesC10H11.9::gfp, pCeh361], qyIs23[P_{cdh-3}::PLC∂PH::mCherry; unc-119(+)]* (Ziel et al., 2009), *zhEx401 [$P_{let-502}$::nls::gfp::lacz::unc-54 3′utr, P_{lin-48}::gfp], zhEx402[$P_{let-502}$ LBS Δ1-4:: nls::gfp::lacz::unc-54 3′utr, P_{lin-48}::gfp], zhEx399[-1.1$P_{let-502}$::nls::gfp::lacz:: unc-54 3′utr, P_{lin-48}::gfp], zhEx403[-2.8$P_{let-502}$ Δ1.1-1.4 kb::nls::gfp::lacz::unc-54 3′utr, P_{lin-48}::gfp], zhEx404[-2.8$P_{let-502}$ Δ1.1-1.8 kb::nls::gfp::lacz::unc-54 3′utr, P_{lin-48}::gfp], zhEx405[-2.8$P_{let-502}$ Δ1.1-2.2 kb::nls::gfp::lacz::unc-54 3′utr, P_{lin-48}::gfp], zhEx393[-2.8$P_{let-502}$ ΔEBS::nls::gfp::lacz::unc-54 3′utr, P_{lin-48}:: gfp], zhEx395[hs::lin-1ΔCT, P_{lin-48}::gfp], zhEx394[hs::3xHA::strep::lin-1ΔCT, P_{lin-48}::gfp], zhIs396[P_{dlg-1}::lifeact::gfp::unc-54 3′utr, P_{lin-48}::gfp], mcEx402 [P_{mlc-4}::gfp::mlc-4DD + P_{pie-1}::gfp::mlc-4(wt), rol-6(gf)]* (Gally et al., 2009), *zhEx398[let-502 genomic, C10H11.8::gfp, P_{lin-48}::gfp], zhEx436[let-502::gfp], sbEx133[P_{mel-11}::gfp, rol-6(su1006)]* (Wissmann et al., 1999), *zhEx439[P_{mlc-4}:: mlc-4RA::gfp], zhEx437[P_{vab-23}::mlc-4RA::gfp], zhEx438[P_{vab-23}::mlc-4DD::gfp]*.

All constructs were microinjected into the gonad arms of adult worms at concentrations between 2 and 50 ng/μl along with the coinjection marker *P_{lin-48}::gfp* at 50 ng/μl and pBluescript added to a final concentration of 150 to 200 ng/μl to generate stable transgenic lines (Mello et al., 1991). Sequences of primers used and details on the construction of plasmids can be found in the Supplemental Experimental Procedures.

RNA Interference

RNA interference (RNAi) was performed using the feeding method as described (Kamath et al., 2001). P0 worms were synchronized at the L1 stage, transferred to nematode growth media plates containing 3 mM IPTG and 50 ng/ml ampicillin seeded with the desired RNAi bacteria, and allowed to grow for 3–5 days at 20°C, after which the surviving F1 progeny was analyzed.

Microscopy and Laser Cutting

Immunostaining was performed as described previously (Miller and Shakes, 1995). In brief, worms were permeabilized using the freeze-crack method and immediately fixed in methanol at −20°C. Samples were blocked with 3% bovine serum albumin, first incubated with primary antibody (1:25 MH27 and 1:1,000 anti NMY-1 or NMY-2) for 2 hr at room temperature, then incubated with secondary antibody (1:100 anti-mouse TRITC and anti-rabbit CY-5), and washed and mounted in Mowiol. Fluorescent images were obtained using a Leica DMRA wide-field microscope, equipped with a cooled CCD camera (Hamamatsu ORCA-ER). Images were analyzed using Openlab 3.0 software package (Improvision). For three-dimensional (3D) reconstructions, GFP and RFP images of larvae animals were recorded with an Olympus FV1000 confocal microscope with a stack size of 0.3 to 0.5 μm. For 4D recordings of vulval toroid morphogenesis, animals were mounted on 4% agarose pads containing 2.5 mM tetramisole and immobilized with 100 nm latex beads (Polysciences Inc.). Images were recorded on an Olympus BX61 DSU spinning disc microscope at 10-min time intervals taking 30 to 40 z-stacks of 0.4 μm per time point. Laser ablation and cutting experiments were performed with a micropoint dye laser (Photonics Instruments) attenuated to around 70% maximal intensity at a pulse rate of 10 Hz aimed at the nucleoli for cell ablations or at the cell extensions to cut the toroids.

Image Analysis

3D reconstructions were made using Imaris software (7.1), and 4D movies were analyzed using Image J. Measurements of toroid height and diameters were conducted on midsagittal sections through the toroids of late L4 larvae, after the VulF lumen had expanded and the AC had fused with the utse. For each parameter, the distances shown in Figure S5 were measured, and the averages and SDs were calculated. Measurements of peak velocities of the VulD recoil were done with Image J using the "kymograph" and "read velocity" macros written by J. Rietdorf and A. Seitz (EMBL Heidelberg).

ChIP Analysis

For ChIP analysis, chromatin was prepared from *hs::HA::lin-1ΔCT* animals and precipitated with anti-HA antibodies (Roche) as described (Mukhopadhyay et al., 2008). As negative control, a mock precipitation using immunoglobulin G as primary antibody was performed in parallel. In each experiment, samples were processed in triplicates. Binding was quantified by Q-PCR with the probes shown in Figure 2A. The primers used for probes are shown in Supplemental Experimental Procedures. For each sample, the signal was normalized to the input DNA (Δct) and the percentage of bound DNA relative to 5% of the input signal was plotted.

SUPPLEMENTAL INFORMATION

Supplemental Information includes five figures, four movies, and Supplemental Experimental Procedures and can be found with this article online at http://dx.doi.org/10.1016/j.devcel.2012.06.019.

ACKNOWLEDGMENTS

We thank Juan Escobar, Stefan Luschnig, Shoib Siddiqui, and Michael Walser for comments on the manuscript, all present and past group members for critical discussion, and Dr. Oleg Georgiev for technical help during cloning. We are

also grateful to Paul Mains and Ken Kemphues for providing NMY antibodies and the *C. elegans* Genetics Centre, S. Mitani (Japan Knockout Consortium), and the Gene Expression Consortium for providing strains and Andrew Fire for vectors. S.F. was the recipient of a Forschungskredit grant from the University of Zürich and travel grants from the Julius Klaus Stiftung and Molecular Life Science PhD Program, Zürich. This research was also supported by the Kanton Zürich and by grants from Swiss National Science Foundation to A.H.

Received: October 7, 2011
Revised: April 6, 2012
Accepted: June 29, 2012
Published online: September 10, 2012

REFERENCES

Abdus-Saboor, I., Mancuso, V.P., Murray, J.I., Palozola, K., Norris, C., Hall, D.H., Howell, K., Huang, K., and Sundaram, M.V. (2011). Notch and Ras promote sequential steps of excretory tube development in *C. elegans*. Development *138*, 3545–3555.

Andrew, D.J., and Ewald, A.J. (2010). Morphogenesis of epithelial tubes: Insights into tube formation, elongation, and elaboration. Dev. Biol. *341*, 34–55.

Beitel, G.J., Tuck, S., Greenwald, I., and Horvitz, H.R. (1995). The *Caenorhabditis elegans* gene *lin-1* encodes an ETS-domain protein and defines a branch of the vulval induction pathway. Genes Dev. *9*, 3149–3162.

Berset, T., Hoier, E.F., Battu, G., Canevascini, S., and Hajnal, A. (2001). Notch inhibition of RAS signaling through MAP kinase phosphatase LIP-1 during *C. elegans* vulval development. Science *291*, 1055–1058.

Brenner, S. (1974). The genetics of *Caenorhabditis elegans*. Genetics *77*, 71–94.

Caussinus, E., Colombelli, J., and Affolter, M. (2008). Tip-cell migration controls stalk-cell intercalation during *Drosophila* tracheal tube elongation. Curr. Biol. *18*, 1727–1734.

Christensen, S., Kodoyianni, V., Bosenberg, M., Friedman, L., and Kimble, J. (1996). lag-1, a gene required for *lin-12* and *glp-1* signaling in *Caenorhabditis elegans*, is homologous to human CBF1 and *Drosophila* Su(H). Development *122*, 1373–1383.

Diogon, M., Wissler, F., Quintin, S., Nagamatsu, Y., Sookhareea, S., Landmann, F., Hutter, H., Vitale, N., and Labouesse, M. (2007). The RhoGAP RGA-2 and LET-502/ROCK achieve a balance of actomyosin-dependent forces in *C. elegans* epidermis to control morphogenesis. Development *134*, 2469–2479.

Estes, K.A., and Hanna-Rose, W. (2009). The anchor cell initiates dorsal lumen formation during *C. elegans* vulval tubulogenesis. Dev. Biol. *328*, 297–304.

Gally, C., Wissler, F., Zahreddine, H., Quintin, S., Landmann, F., and Labouesse, M. (2009). Myosin II regulation during *C. elegans* embryonic elongation: LET-502/ROCK, MRCK-1 and PAK-1, three kinases with different roles. Development *136*, 3109–3119.

Gov, N.S. (2007). Collective cell migration patterns: follow the leader. Proc. Natl. Acad. Sci. USA *104*, 15970–15971.

Greenwald, I. (2005). LIN-12/Notch signaling in *C. elegans*. WormBook, 1–16.

Herman, T., and Horvitz, H.R. (1999). Three proteins involved in *Caenorhabditis elegans* vulval invagination are similar to components of a glycosylation pathway. Proc. Natl. Acad. Sci. USA *96*, 974–979.

Herman, T., Hartwieg, E., and Horvitz, H.R. (1999). *sqv* mutants of *Caenorhabditis elegans* are defective in vulval epithelial invagination. Proc. Natl. Acad. Sci. USA *96*, 968–973.

Hwang, H.Y., Olson, S.K., Esko, J.D., and Horvitz, H.R. (2003). *Caenorhabditis elegans* early embryogenesis and vulval morphogenesis require chondroitin biosynthesis. Nature *423*, 439–443.

Ihara, S., Hagedorn, E.J., Morrissey, M.A., Chi, Q., Motegi, F., Kramer, J.M., and Sherwood, D.R. (2011). Basement membrane sliding and targeted adhesion remodels tissue boundaries during uterine-vulval attachment in *Caenorhabditis elegans*. Nat. Cell Biol. *13*, 641–651.

Jacobs, D., Beitel, G.J., Clark, S.G., Horvitz, H.R., and Kornfeld, K. (1998). Gain-of-function mutations in the *Caenorhabditis elegans lin-1* ETS gene identify a C-terminal regulatory domain phosphorylated by ERK MAP kinase. Genetics *149*, 1809–1822.

Kamath, R.S., Martinez-Campos, M., Zipperlen, P., Fraser, A.G., and Ahringer, J. (2001). Effectiveness of specific RNA-mediated interference through ingested double-stranded RNA in *Caenorhabditis elegans*. Genome Biol. *2*, RESEARCH0002.

Köppen, M., Simske, J.S., Sims, P.A., Firestein, B.L., Hall, D.H., Radice, A.D., Rongo, C., and Hardin, J.D. (2001). Cooperative regulation of AJM-1 controls junctional integrity in *Caenorhabditis elegans* epithelia. Nat. Cell Biol. *3*, 983–991.

Lackner, M.R., and Kim, S.K. (1998). Genetic analysis of the *Caenorhabditis elegans* MAP kinase gene *mpk-1*. Genetics *150*, 103–117.

Lints, R., and Hall, D.H. (2009). Reproductive system, egglaying apparatus In WormAtlas. http://dx.doi.org/10.3908/wormatlas,1.24.

Lundquist, E.A., Reddien, P.W., Hartwieg, E., Horvitz, H.R., and Bargmann, C.I. (2001). Three *C. elegans* Rac proteins and several alternative Rac regulators control axon guidance, cell migration and apoptotic cell phagocytosis. Development *128*, 4475–4488.

Mello, C.C., Kramer, J.M., Stinchcomb, D., and Ambros, V. (1991). Efficient gene transfer in *C.elegans*: extrachromosomal maintenance and integration of transforming sequences. EMBO J. *10*, 3959–3970.

Miller, D.M., and Shakes, D.C. (1995). Immunofluorescence microscopy. Methods Cell Biol. *48*, 365–394.

Miller, L.M., Gallegos, M.E., Morisseau, B.A., and Kim, S.K. (1993). *lin-31*, a *Caenorhabditis elegans* HNF-3/fork head transcription factor homolog, specifies three alternative cell fates in vulval development. Genes Dev. *7*, 933–947.

Mukhopadhyay, A., Deplancke, B., Walhout, A.J., and Tissenbaum, H.A. (2008). Chromatin immunoprecipitation (ChIP) coupled to detection by quantitative real-time PCR to study transcription factor binding to DNA in *Caenorhabditis elegans*. Nat. Protoc. *3*, 698–709.

Omelchenko, T., Vasiliev, J.M., Gelfand, I.M., Feder, H.H., and Bonder, E.M. (2003). Rho-dependent formation of epithelial "leader" cells during wound healing. Proc. Natl. Acad. Sci. USA *100*, 10788–10793.

Pellegrino, M.W., Farooqui, S., Fröhli, E., Rehrauer, H., Kaeser-Pebernard, S., Müller, F., Gasser, R.B., and Hajnal, A. (2011). LIN-39 and the EGFR/RAS/MAPK pathway regulate *C. elegans* vulval morphogenesis via the VAB-23 zinc finger protein. Development *138*, 4649–4660.

Piekny, A.J., Johnson, J.L., Cham, G.D., and Mains, P.E. (2003). The Caenorhabditis elegans nonmuscle myosin genes *nmy-1* and *nmy-2* function as redundant components of the *let-502*/Rho-binding kinase and *mel-11*/myosin phosphatase pathway during embryonic morphogenesis. Development *130*, 5695–5704.

Pohl, C., and Bao, Z. (2010). Chiral forces organize left-right patterning in *C. elegans* by uncoupling midline and anteroposterior axis. Dev. Cell *19*, 402–412.

Poujade, M., Grasland-Mongrain, E., Hertzog, A., Jouanneau, J., Chavrier, P., Ladoux, B., Buguin, A., and Silberzan, P. (2007). Collective migration of an epithelial monolayer in response to a model wound. Proc. Natl. Acad. Sci. USA *104*, 15988–15993.

Rodríguez-Fraticelli, A.E., Gálvez-Santisteban, M., and Martín-Belmonte, F. (2011). Divide and polarize: recent advances in the molecular mechanism regulating epithelial tubulogenesis. Curr. Opin. Cell Biol. *23*, 638–646.

Sapir, A., Choi, J., Leikina, E., Avinoam, O., Valansi, C., Chernomordik, L.V., Newman, A.P., and Podbilewicz, B. (2007). AFF-1, a FOS-1-regulated fusogen, mediates fusion of the anchor cell in *C. elegans*. Dev. Cell *12*, 683–698.

Schottenfeld, J., Song, Y., and Ghabrial, A.S. (2010). Tube continued: morphogenesis of the *Drosophila* tracheal system. Curr. Opin. Cell Biol. *22*, 633–639.

Sementchenko, V.I., and Watson, D.K. (2000). Ets target genes: past, present and future. Oncogene *19*, 6533–6548.

Sharma-Kishore, R., White, J.G., Southgate, E., and Podbilewicz, B. (1999). Formation of the vulva in *Caenorhabditis elegans*: a paradigm for organogenesis. Development *126*, 691–699.

Sternberg, P.W. (2005). Vulval development. WormBook, 1–28.

Tan, P.B., Lackner, M.R., and Kim, S.K. (1998). MAP kinase signaling specificity mediated by the LIN-1 Ets/LIN-31 WH transcription factor complex during *C. elegans* vulval induction. Cell *93*, 569–580.

Vaughan, R.B., and Trinkaus, J.P. (1966). Movements of epithelial cell sheets in vitro. J. Cell Sci. *1*, 407–413.

Wissmann, A., Ingles, J., McGhee, J.D., and Mains, P.E. (1997). *Caenorhabditis elegans* LET-502 is related to Rho-binding kinases and human myotonic dystrophy kinase and interacts genetically with a homolog of the regulatory subunit of smooth muscle myosin phosphatase to affect cell shape. Genes Dev. *11*, 409–422.

Wissmann, A., Ingles, J., and Mains, P.E. (1999). The *Caenorhabditis elegans mel-11* myosin phosphatase regulatory subunit affects tissue contraction in the somatic gonad and the embryonic epidermis and genetically interacts with the Rac signaling pathway. Dev. Biol. *209*, 111–127.

Xavier Trepat, M.R.W., Angelini, T.E., Millet, E., Weitz, D.A., Butler, J.P., and Fredberg, J.J. (2009). Physical forces during collective cell migration. Nat. Phys. *5*, 426–430.

Zhang, X., and Greenwald, I. (2011). Spatial regulation of *lag-2* transcription during vulval precursor cell fate patterning in *Caenorhabditis elegans*. Genetics *188*, 847–858.

Ziel, J.W., Hagedorn, E.J., Audhya, A., and Sherwood, D.R. (2009). UNC-6 (netrin) orients the invasive membrane of the anchor cell in *C. elegans*. Nat. Cell Biol. *11*, 183–189.